Journal of Polymers and the Environment (2022) 30:2493–2506
https://doi.org/10.1007/s10924-021-02357-2

ORIGINAL PAPER

Optimization and Characterization of Bioactive Biocomposite Film Based on Orange Peel Incorporated with Gum Arabic Reinforced by Cr_2O_3 Nanoparticles

Saba Ghasemizad[1] · Sajad Pirsa[2] · Saber Amiri[2] · Parisa Abdosatari[2]

Accepted: 6 December 2021 / Published online: 15 January 2022

Abstract

In this paper, the effect of adding gum arabic at levels of 0–5%, and chromium oxide nanoparticles (Cr_2O_3 NPs) at levels of 0–3%, were optimized on orange peel-based films by response surface methodology. The obtained results reveal a significant increase in water vapor permeability, weight loss, tensile strength, and Young's modulus of film samples by increasing the percentage of both gum and nanoparticles ($p < 0.05$). Moreover, the addition of gum arabic and Cr_2O_3 NPs decreases the thickness, water-solubility, L^*, a^*, b^* indexes while increasing the elongation to the breaking point. Furthermore, the moisture content of the film samples was decreased by the addition of nanoparticles, however, the addition of gum arabic increased this parameter. The obtained results from the morphology of the samples indicated an increase in both roughness and cracks by increasing the percentage of nanoparticles as well as creating a smooth surface with the addition of gum arabic. Besides, the results of Fourier-transform infrared spectroscopy revealed no new peak in the prepared samples, as compared to the control sample. The results of X-ray diffraction indicated that the addition of gum arabic and nanoparticles simultaneously caused the formation of new crystals and increasing the crystallinity of the films. Based on Thermogravimetric analysis results, the thermal stability of films containing the nanoparticles increased, as compared to the control sample. In the meantime, the addition of gum and nanoparticles increased the antimicrobial properties of the film samples, as compared to the control. Overall, those films created by the orange peel including gum arabic and Cr_2O_3 NPs could enhance the mechanical properties and water vapor permeability of the samples.

Keywords Biodegradable film · Orange peel powder · Acacia gum · Cr_2O_3 nanoparticles · Central composite design

Introduction

Plastic, well-known as one of the best human products, has now become a major challenge for both the environment and humans since it is an indestructible material with a shelf life of approximately 300 years. Here, it should be mentioned that the big volume of discarded plastics resultant from the packaging of food and hygiene products, now has created several problems, the most obvious of which is the irreparable damage to water, soil, air, and creatures [1].

By increasing the population as well as pressure on the restricted resources and the environment, the use of renewable resources to produce edible and biodegradable films has become increasingly important, which can improve product quality or decrease the waste disposal problems [2, 3]. Antimicrobial packaging as an active packaging type is one of the packages, which has recently been widely used to increase the shelf life of food [4, 5]. Antimicrobial food packaging acts to inhibit or delay the growth of microorganisms possibly existing in the food package or the packaged food. Metal oxide nanoparticles are among the compounds used in the antimicrobial packaging, among which, special attention has been paid to the formation and properties of chromium (Cr_2O_3), as an important heterogeneous coating

✉ Sajad Pirsa
pirsa7@gmail.com; s.pirsa@urmia.ac.ir

✉ Saber Amiri
sa.amiri@urmia.ac.ir

[1] Department of Food Science and Technology, Faculty of Agriculture, Saba Institute of Higher Education, Urmia, Iran

[2] Department of Food Science and Technology, Faculty of Agriculture, Urmia University, P.O. Box, 57561-51818 Urmia, Iran

material, abrasion-resistant catalyst, solar energy storage, and high coloring.

Gums are one of the natural polymers that are recently utilized to synthase the packaging materials. Gums or hydrocolloids have been used since 5000 years ago [6, 7]. They are generally consumed in the food industry to change the texture, rheological properties and preserve the appearance of food as a result of their ability to stabilize emulsions and water storage [8]. Gum Arabic is one of the types of hydrocolloids, which is the best type of gum because of its emulsification and encapsulation properties for use in oil-in-water emulsion systems [9]. Other advantages of gum arabic include its cost-effectiveness, high concentration, and widespread use of various products [10].

Orange fruit is widely used around the world as fresh produce and juice. Its peel is often discarded as waste, which includes insoluble fibers (cellulose, hemicellulose and lignin), soluble fiber (pectin), and various secondary compounds with antioxidant and antimicrobial properties (limonene, myrcene, α-farnesene, γ-terpinene, α-pinene, β-pinene, and α-terpinolene). There has been an increasing interest in the incorporation of biofiller from low economic value by-products in biocomposites as natural additives to improve the functionality of biopolymer packaging materials. Orange peels are promising biofiller candidates for biocomposites production. This biofiller is widely available, cost-effective, and biodegradability, which can propose great opportunities to improve value-added and environmentally friendly structural composites from waste [11–13].

In this paper, the orange peel powder was used as base component to prepare the packaging film. For this purpose, the effect of gum arabic and chromium oxide nanoparticles (Cr_2O_3 NPs) concentrations on phsical, barrier, and appearance properties of biodegradable film based on orange peel was optimized. Then the mechanical, structural, thermal, and morphological properties of optimizd active films were characterized.

Materials and Methods

Materials

The oranges (Valencia cultivar) were bought from the local market of Urmia, Iran. Gum Arabic, Cr_2O_3 NPs, corn starch, glycerol, calcium nitrate, calcium sulfate, potassium sulfate, sodium hydroxide, sodium chloride, and methanol 99.8% were from Merck (Darmstadt, Germany). 2,2-diphenyl-1-picrylhydrazyl (DPPH) was made by Sigma-Aldrich (St. Louis, MO, USA). The Nutrient agar culture medium was bought from the Merck (Darmstadt, Germany). Moreover, the standard strains of *Staphylococcus aureus* PTCC 1431 and *Escherichia coli* PTCC 1763 were purchased from the Iran Industrial and Scientific Research Organization, Tehran, Iran.

Preparing Orange Peel Powder (OPP)

The orange peel was dried at room temperature after washing and ground. After sieving, the resulting powder was covered in a plastic bag and was stored in the refrigerator [14].

Film Preparation

At first, two grams of orange peel were dispersed in 100 mL of distilled water and then stirred for 20 h on a heated mixer at 30 °C at 250 RPM. Then, after 20 h, 40% glycerol (based on the dry weight of orange peel) was added and stirred again for 30 min. In the end, after filtration, the prepared solution was poured into 35 mL plates and then dried at room temperature [14].

Film Characteristics

Thickness

The film thickness was measured using a digital micrometer at five random points of each film (around and center of each film). Afterward, the average thickness of different points of each film was utilized to calculate the mechanical properties and water vapor permeability [15].

Weight Loss Percentage

To measure the weight loss of the films, small pieces of the film were dried in an oven at 105 °C for 24 h. Then, the weight of the films was recorded before and after drying in the oven. The amount of weight loss was then calculated as the percentage of initial weight loss as follows:

$$\text{Weight loss} = \frac{(W_0 - W1)}{W_0} \quad (1)$$

where W_0 means the initial dry weight, W_1 represents the final dry weight [16].

Measuring the Moisture Content of the Films

The films were cut into 2 × 2 cm and then weighed carefully. Afterward, they were placed in aluminum dishes and dried in an oven at 105 °C for 24 h. The moisture content was calculated based on the difference between the initial and final weight of the samples [17].

Water Solubility

To measure the water solubility of the films, the film samples were prepared in 2 × 2 cm. They were placed in an oven at 110 °C for 6 h to obtain the initial dry weight. After weighing (W_1), the samples were immersed in the sealed dishes containing 50 mL of distilled water. The dishes were stirred as cross-sectional at 25 °C for 18 h. Then, the films were removed from the water and again placed in an oven at 110 °C for 6 h to achieve a constant weight. By re-weighing, the samples, the final dry weight (W_2) was obtained. The percentage of water solubility was calculated as follows [18]:

$$\%WS = \frac{W_1 - W_2}{W_1} \times 100 \quad (2)$$

where W_1 is the initial dry weight and W_2 denotes the final dry weight.

Measuring Water Vapor Permeability (WVP)

ASTM E96-05 method is employed to measure water vapor transfer (ASTM, 2005) using the special vials. There was a 5 mm diameter hole in the lid of these vials, in which a piece of film was placed. Then, 3 g of calcium sulfate was placed in vials. A piece of film was cut and then placed in the lid of the vial, and closed on the vial. The vials were weighed with all the contents and then placed in a desiccator containing a saturated solution of potassium sulfate. To ensure saturation, some precipitate of potassium sulfate was allowed to form on the bottom of the desiccator. Saturated potassium sulfate at 25 °C produces a relative humidity of 97%. Then, the weight of the vials was measured every 4 days for several hours.

The amount of water vapor transferred from the films was determined by increasing the weight of the vials. The weight gain curve of the vials over time was plotted, and after calculating the linear regression, the slope of the resulting line was calculated. Dividing the slope of the line associated with each vial by the total surface area of the film exposed to water vapor transfer, the water vapor transfer rate (WVTR) is obtained. The water vapor permeability (WVP) was then calculated as follows:

$$WVP = \frac{WVTR}{P(R_1 - R_2)}.X \quad (3)$$

where X means the film thickness (m), P denotes the pure water vapor pressure at 25 °C (3169 Pa), R_1 refers to the relative moisture in the desiccator (97%), and R_2 is the relative moisture inside the vial (0%). The test was implemented on each sample in three repetitions.

Measuring Color Properties

A Colorimeter Minolta (Model CR-410, Tokyo, Japan) was employed to specify the surface color of the film samples. The results were exhibited in light–dark (L^*), green–red (a^*), and blue-yellow (b^*) [19]. Besides, the whiteness index (WI) and Chroma (C^*) were calculated using the following equations:

$$WI = 100 - \sqrt{(100 - L^*)^2 + a^{*2} + b^{*2}} \quad (4)$$

$$\text{Chroma} = \sqrt{(a^*)^2 + (b^*)^2} \quad (5)$$

Measuring Mechanical Properties

The mechanical properties of the film samples were specified using the tensile tests by a Texture Analyzer (TA.XT plus texture analyser, Stable Micro systems, UK) based on the instructions of the ASTM D882-10 standard method. To implement the tensile test, the samples (with two replication for each sample) were conditioned in a desiccator including the magnesium nitrate saturated solution with relative moisture of 50 ± 5% for 24 h. Then, they were cut into rectangular strips, and both longitudinal ends of each film were placed between the two jaws of the device [20]. By initiating the test operation, the film was pulled between the two jaws until it was torn, based on which the work process appeared as a stress–strain diagram. The tensile strength, elongation at the breaking point, and the modulus of elasticity properties of the films were calculated as follows:

$$\text{Ultimate tensile strength} = \frac{F_{max}}{A} \quad (6)$$

$$\text{Elongation at break} = \frac{L_{max}}{L_0} \times 100 \quad (7)$$

$$\text{Young's modulus} = \frac{(F.L_0)}{(A.\Delta L)} \quad (8)$$

where A represents the film cross-sectional area (m^2), F_{max} denotes the maximum force at the breakpoint (N), L_{max} means the film elongation at the breakpoint (m), L_0 is the initial length of film sample (m), F is the force (N) and ΔL represents the changes in the length of the sample to the breaking point (m).

Field Emission Scanning Electron Microscopy

To evaluate the morphology, the surface of the film samples was examined using a Field emission scanning electron

microscope (SIGMA VP, ZEISS, Germany) at room temperature. Before scanning, a gold coating in several nanometers thickness was coated on the fracture surfaces [21].

Fourier Transform Infrared Spectroscopy (FT-IR) Test

FT-IR (Spectrum two, Perkin Elmer, USA) was utilized in the range of 400–4000 cm^{-1} with a resolution of 4 cm^{-1} to survey the interactions in the film matrix. First, the device was zeroed with KBr tablet as a control sample, and then the samples were prepared for FT-IR analysis by mixing 1 mg of completely dried samples via 150 mg of dry KBr powder. The thin tablets were prepared from each sample by compressing the mixture in a press device [22].

X-Ray Diffraction Test

X-ray diffraction pattern of the film samples was employed to investigate the crystal structure of the prepared films and determine the distribution of components in the polymer matrix using Siemens, model D5005, Baden-wurttemberg, Germany [23].

Thermogravimetric Analysis

The dried film samples were analyzed from 20 to 500 °C at a heating rate of 10 °C/min along with the pure nitrogen gas at a rate of 20 mm/min using Linseis model Sta Pt-1000, Germany [23].

Investigating Antimicrobial Properties of the Films

To determine the antimicrobial properties of active films, the method of penetration of antimicrobial compounds in agar medium (every 4 days) was utilized. In this method, the films were cut into circular plates and then transferred to the nutrient agar culture medium, which was previously inoculated with 10^5–10^6 CFU/mL of *Escherichia coli* (*E. coli*) or *Staphylococcus aureus* (*S. aureus*) microorganisms. After that, petri dishes comprising the contaminated culture medium along with antimicrobial films were kept in an incubator at 37 °C for 24 h. To obtain the degree of the microorganisms growth inhibition by the film, the diameter of the growth inhibition zone formed around the films was measured using a caliper [24].

Statistical Analysis

In this paper, the effect of two numerical factors on the concentration of gum arabic (0%, 2.5%, and 5%) and Cr_2O_3 NPs (0%, 1.5%, and 3%) are investigated using the response surface methodology in the form of a central composite design. In this design, 13 samples (including 4 factorial points, 4 axial points, and 5 central points are considered to estimate the mismatching and reproducibility). After implementing the experiments and data collection to test the significance of the factors and their interactions, the method of analysis of variance (ANOVA) and Fisher distribution was employed at the significance level of $\alpha = 0.05$. The software Design-expert (version 11, StatEase Inc., Minneapolis, MN, USA) was utilized to analyze the data and draw the graphs.

Results and Discussion

Thickness

The results indicated that by increasing the percentage of Cr_2O_3 NPs, the film thickness decreased, whereas the addition of gum arabic had little effect on the film sample thickness (Fig. 1). Overall, those films via the highest levels of nanoparticles and gum had the highest thickness, which might be due to the increase in the solid materials [25]. The reason for the thickness reduction behavior through increasing the nanoparticle percentage is also related to the increased density in the polymer film structure by the Cr_2O_3 NPs. According to the results of several researchers, it can be concluded that the thickness of the films changes based on the type of polymer and the added nanoparticles, and can cause the thickness to decrease, increase, or remain constant.

Weight Loss

Figure 2 illustrates the three-dimensional curve of the film weight loss percentage. By increasing the gum content

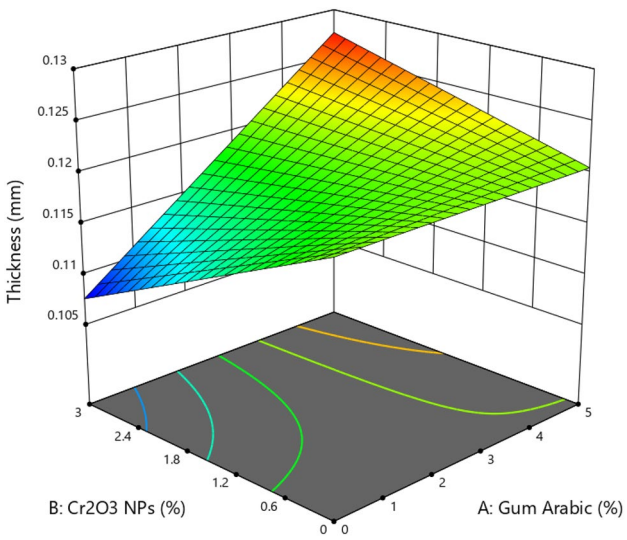

Fig. 1 The three-dimensional curve of the effect of nanoparticle-gum percentage on the thickness of films

percentage, the film weight loss percentage reduced while increasing the Cr_2O_3 NPs, it was increased significantly ($p < 0.05$). It should be noted that those samples containing the highest levels of nanoparticles and no gum arabic had the highest weight loss. Moreover, the effect of the second-degree percentage of gum and Cr_2O_3 NPs on weight loss was also significant.

Measuring the Moisture Content of the Films

Figure 3 depicts the three-dimensional curve of the effect of gum and Cr_2O_3 NPs percentage on the amount of moisture. It should be mentioned that by increasing the percentage of gum, the moisture content of the film increased, while by increasing the percentage of Cr_2O_3 NPs, the moisture content of the film significantly decreased ($p < 0.05$).

Besides, the moisture content of the film increased by increasing the gum. This seems to be due to the increased compression of the film matrix and the entrapment of more water in the film matrix structure. On the other hand, high hydrophilicity of the gum cause more water absorption by the gum and thus increasing the moisture content of the films [26]. Furthermore, the reduction in the moisture content with the addition of nanoparticles is likely due to the weak interaction of nanoparticles with the hydroxyl polymer group [25]. Our results in terms of the effect of adding nanoparticles on reducing the moisture content of films are in accordance with the results of Li et al. [27] who added zinc oxide nanoparticles to chitosan, as well as Bahrami et al. [25] adding the silver nanoparticles to the films based on hydroxypropyl methylcellulose and Tragacanth.

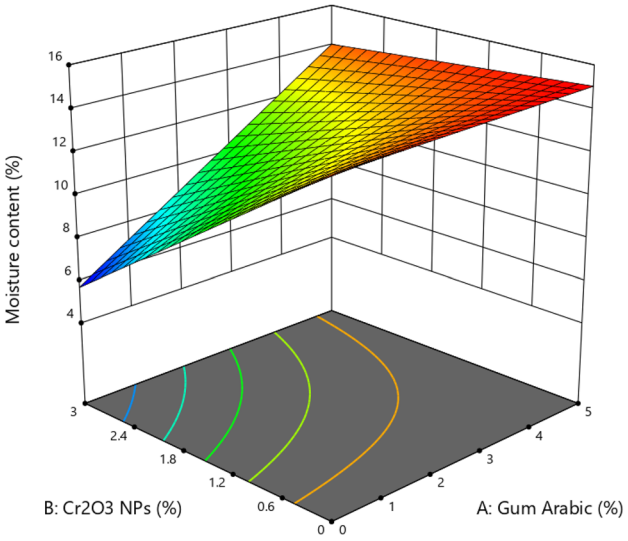

Fig. 3 The three-dimensional curve of the effect of nanoparticle-gum percentage on the moisture content of the films

Water Solubility

Figure 4 exhibits the three-dimensional curve of the film solubility as a function of two variables of the gum and Cr_2O_3 NPs percentages. The obtained results revealed that by increasing the percentage of gum and Cr_2O_3 NPs, the solubility of the film decreased. Note that the second-degree effect of gum and the linear effect of Cr_2O_3 NPs were also significant.

Here, it is worth noting that solubility is an essential feature in biodegradable films because it can resist the film

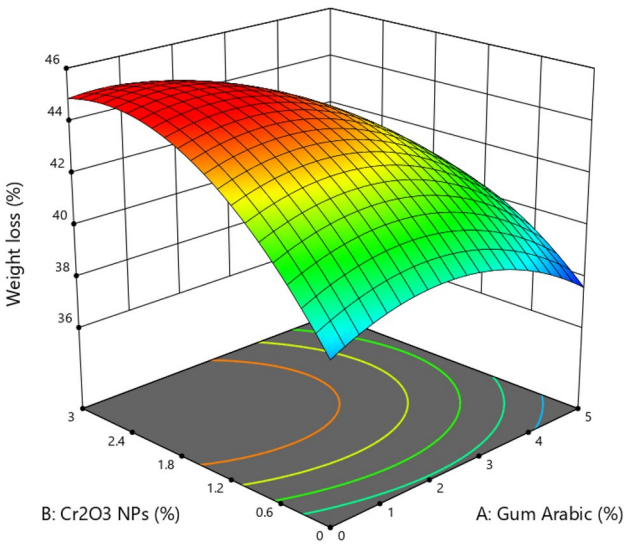

Fig. 2 The three-dimensional curve of the effect of nanoparticle-gum percentage on the percentage of weight loss of films

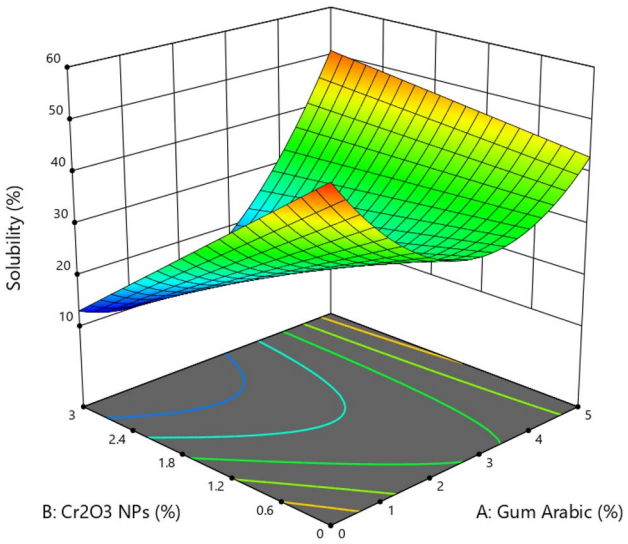

Fig. 4 A three-dimensional curve of the percentage of nanoparticle-gum on the water solubility of films

compared to water, especially in the environment containing moisture such as meat products, and determine the release speed of antioxidant and antimicrobial compounds when in contact with the material food. Adding the nanoparticles increases the electrostatic bonding between film polymer, and thus decreasing the water solubility of the film. Some similar results are provided by adding clay nanoparticles to the film based on pectin [28]. Rezaei et al. [29] reported that the addition of zinc oxide nanoparticles reduced the water solubility of the films. Our results in terms of the effect of gum on reducing water solubility were in accordance with the result of Sui et al. [30]. They found reduced water solubility by increasing the amount of Tragacanth. Khoirunnisa et al. [31] expressed that the addition of zinc nanoxide led to a significant change in the solubility of the films, which was consistent with our findings in terms of the effect of nanoparticles on reducing the water solubility of film.

They described this phenomenon attributed to the possible bonding between nanoparticles and film matrix. Some studies revealed that the addition of nanoparticles causes hydrogen bonding between nanoparticles and polymer matrix. As such, the bonding of free molecules of water and hydrophilic biopolymer groups reduced, and subsequently, the film solubility decreased [32].

Measurement of Water Vapor Permeability (WVP)

Figure 5 illustrates the three-dimensional curve of water vapor permeability (WVP) as a function of two variables of gum and Cr_2O_3 NPs. The results of the statistical analysis confirmed that by increasing Cr_2O_3 NPs, the amount of WVP increases significantly. Moreover, by increasing the gum surfaces, the amount of WVP of the samples decreased, and then slightly increased.

Furthermore, the second-degree effect of gum and Cr_2O_3 NPs was significant on WVP ($p < 0.05$). Note that increasing the WVP of the films by adding nanoparticles, is due to porous structure and gaps caused by nanoparticles [33]. Similar results were obtained for films comprising *Gracilaria vermiculophylla* extract and zinc oxide nanoparticles [33].

Measuring Color Properties

The color and appearance of the polymer used in food packaging is an essential and effective factor for choosing and accepting the product by the consumer. Most food packaging films are transparent and colorless. Nevertheless, in some cases, the use of the inhibitor compounds of light, and generating the color in the matrix of the packaging material are necessary, due to the sensitivity of food to light, the loss of its nutritional compounds by optical oxidation, and color matching contents with packaging material to attract the consumer attention [34].

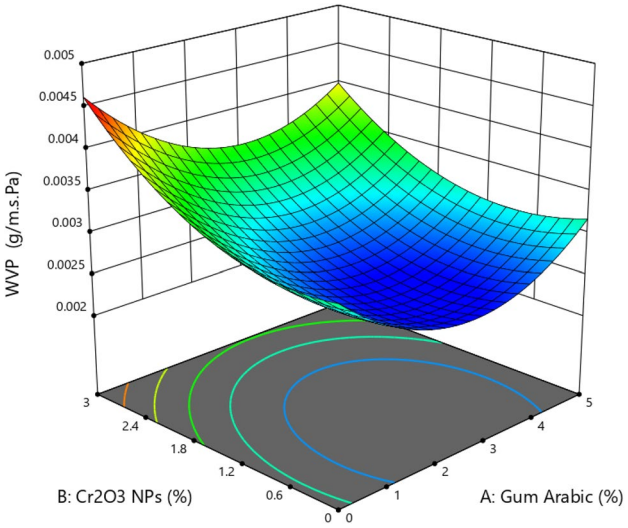

Fig. 5 A three-dimensional curve of the percentage of nanoparticle-gum on the water vapor permeability of the films

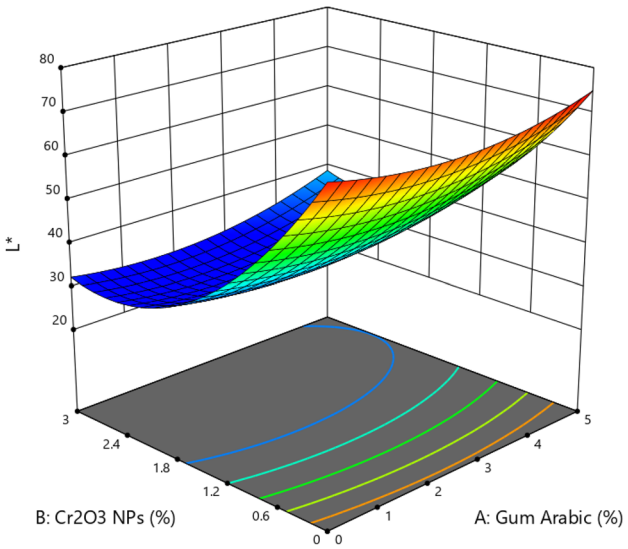

Fig. 6 A three-dimensional curve of the percentage of nanoparticle-gum on the L^* index of films

Figure 6 depicts the three-dimensional curve of film lightness (L^*) as a function of two variables of gum and Cr_2O_3 NPs percentages. The obtained results of the statistical analysis revealed that by increasing the gum percentage, the film L^* increased; however, by increasing the percentage of Cr_2O_3 NPs, the amount of the film L^* decreases significantly.

Sui et al. [30] indicated that the higher the ratio of gum to soy protein isolate, the brighter the color of the film will be. This is in line with our results revealing the increased L^* along with increasing the gum. As can be observed, by increasing nanoparticles, the transparency of the films

decreases, which was in accordance with the results of Jabraili et al. [35]. They described that by increasing the number of nanofibers, the transparency of polylactic acid films decreased. Besides, the decrease in L^* with the addition of nanoparticles may be due to the matte appearance of Cr_2O_3 NPs [25].

Figure 7 exhibits the three-dimensional curve of the a^* index of the film as a function of two variables of gum and Cr_2O_3 NPs. The results indicated that by increasing the gum percentage, the value of a^* index increased, while by increasing the Cr_2O_3 NPs, the a^* index content of the films decreased.

In terms of the effect of nanoparticles, it could be seen that by adding nanoparticles, the value of a^* was reduced, which was consistent with the results of Oleyaei et al. [26].

Figure 8 illustrates the three-dimensional curve of the b^* index of the film as a function of two variables of gum and Cr_2O_3 NPs. The results of statistical analysis indicated that by increasing the percentage of gum, the amount of b^* index of the film increased, while by increasing the percentage of Cr_2O_3 NPs, the b^* index of the film significantly decreased. Considering the effect of nanoparticles, it can be observed that by the addition of nanoparticles, the b^* was decreased, which was in line with the results of Oleyaei et al. [26].

Figure 9 depicts a three-dimensional whiteness index (WI) as a function of two variables of gum and Cr_2O_3 NPs percentage. The obtained results confirmed that the WI rate increased by increasing the percentage of gum, whereas by increasing the Cr_2O_3 NPs, the WI decreased.

Figure 10 exhibits the three-dimensional curve of the film as a function of two variables of gum and Cr_2O_3 NPs percentage. The statistical analysis revealed that by

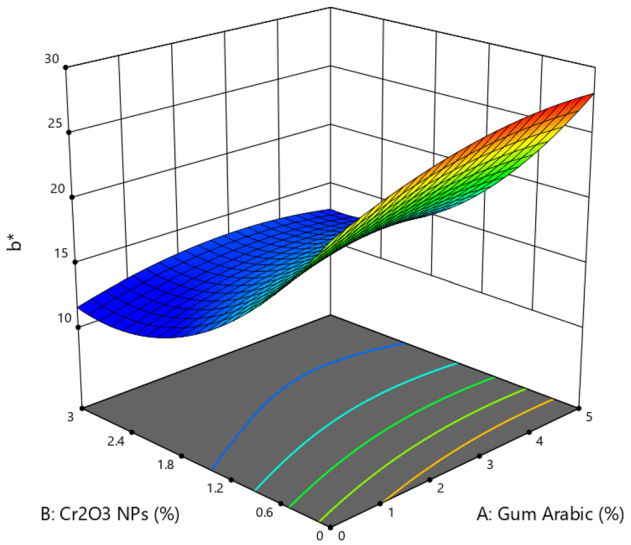

Fig. 8 A three-dimensional curve of the percentage of nanoparticle-gum on the parameter b^* index films

increasing the gum percentage, the amount of C^* index in the film increased, while by increasing the percentage of Cr_2O_3 NPs, the film C^* significantly decreased ($p < 0.05$). The C^* denotes a measure of a color difference of gray, which can be defined as color purity. The calculation of the amount of C^* in the samples shows the highest amount of purity in the film samples. The results in this regard were consistent with the results of He et al. [36]. They provided that with the addition of oxide nanoparticles, the amount of C^* decreased.

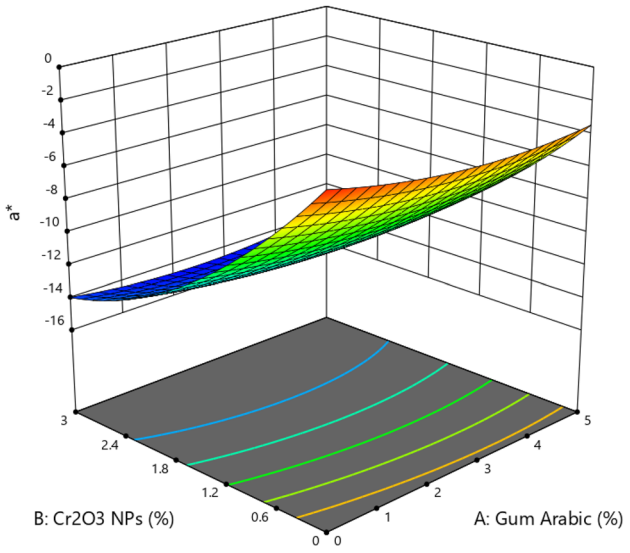

Fig. 7 A three-dimensional curve of the percentage of nanoparticle-gum on the parameter a^* index films

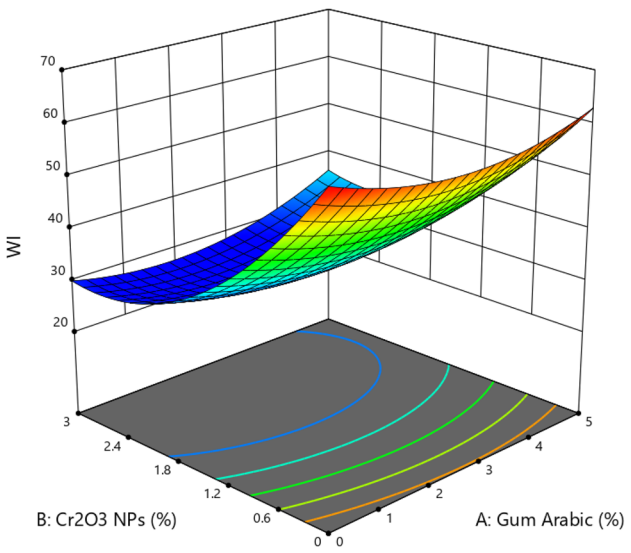

Fig. 9 A three-dimensional curve for the effect of the percentage of nanoparticle-gum on the WI of films

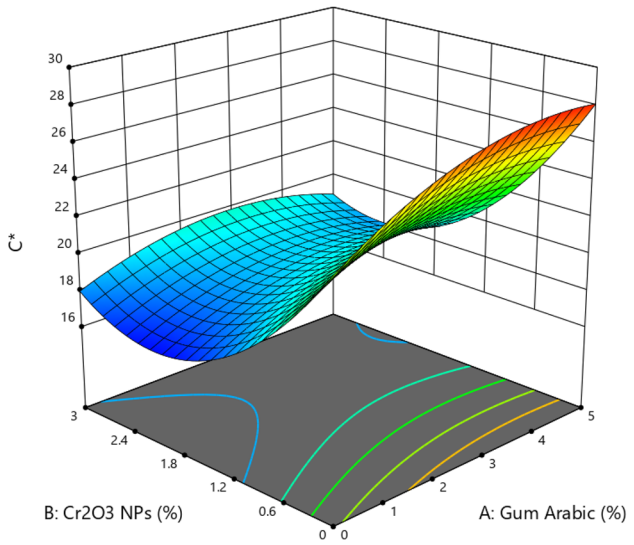

Fig. 10 The three-dimensional curve of the nanoparticle-gum percentage on *C** index of films

Table 1 The data on the mechanical properties of films based on orange peel and gum arabic

Sample	% E	YM (MPa)	TS (MPa)
OPP	21.62 ± 0.88^{a}	34.07 ± 1.21^{c}	7.34 ± 0.10^{c}
OPP/AG	17.69 ± 0.67^{b}	60.41 ± 4.36^{a}	10.63 ± 0.39^{a}
OPP/Cr_2O_3	21.29 ± 0.13^{a}	50.54 ± 0.73^{b}	10.76 ± 0.18^{a}
OPP/Cr_2O_3/AG	20.95 ± 0.83^{a}	41.98 ± 2.10^{c}	8.76 ± 0.20^{b}

Different letters in each column indicate significance at the level of $p < 0.05$

Measuring Mechanical Properties

Mechanical properties are considered the most important properties of materials used in food packaging. Among the important mechanical properties of biodegradable films are the tensile strength and tensilability to the breaking point to determine their resistances in different processes, transportation, and warehousing.

Table 1 lists the percentage of elongation, tensile strength, and elastic modulus of samples 6, 8, 12 against the control sample (sample 13). As can be observed, by adding the gum arabic and nanoparticles in samples 6 and 12, the tensile resistance parameter has a significant increase, as compared to the control sample. This can be associated with the creation of appropriate interactions between film matrix and additive materials (such as gum arabic and Cr_2O_3 NPs), where this parameter increased by forming new hydrogen bonding. Furthermore, the uniformity of nanoparticles in the films increases the tensile strength, as compared to the control sample [37]. Moreover, the modulus of the elasticity reveals the same process and indicates the creation of interactions in the film matrix. This is in line with the results of Xu et al. [11] in terms of the addition of the ZnO-CMC combined nanoparticles to the pea starch film. Besides, He et al. [36] proposed that two parameters of elasticity modulus and tensile strength were increased by adding the zinc nanoxide to the gelatin fish.

In this matter, the addition of titanium oxide and silver nanoparticles to the Carboxymethyl cellulose film increased both the tensile strength and modulus of elasticity [37]. However, in sample 8 (i.e. the sample including the highest percentage of gum arabic and chromium oxide), it can be seen the decrease in these two parameters can be associated with the lack of adequate interactions with the film matrix and the formation of bonding between nanoparticles and gum. In other words, instead of the formation of abundant hydrogen bonding with film matrix, nanoparticles and gum create abundant hydrogen bonding with each other, which finally would result in reducing the tensile strength elasticity modulus. Meanwhile, there was no logical process for the percentage of elongation (% E).

Field Emission Scanning Electron Microscopy (FE-SEM)

The analysis of the film's morphology provides information on the spatial layout of different components in the film, which helps understand the mechanical properties and water vapor transfer mechanisms [38]. In this regard, the SEM images resulting from the sample surface of the films are depicted in Fig. 11. The SEM images show the control film based on the dense and uniform surface of orange peel (Fig. 11a). As can be observed from Fig. 11b, Cr_2O_3 NPs were uniformly distributed without agglomeration of particles at the surface of the film sample. Besides, as compared to the control sample, adding nanoparticles to films caused rough surfaces, more cracks, and a break at the surface of the film samples.

Oun and Rhim [39] reported the uniform distribution of zinc oxide nanoparticles in carrageenan films. Based on Fig. 11c, the addition of gum arabic to orange peel films caused a uniform surface with no fracture. This condition may be resultant due to intra-molecular interaction between polymer matrix. In this regard, the results of coordination were achieved for those films based on carrageenan gum, Xanthan Gum, and Gellan gum, which were prepared with different proportions [40].

In the images related to films containing 5% gum and 3% of Cr_2O_3 NPs, surface with more and deeper cracks and fractures, and more non-uniformity can be seen, as compared to the control sample. Besides, they had a non-homogeneous surface than the control film (Fig. 11d). These results are probably due to the interaction between polymer, gum, and

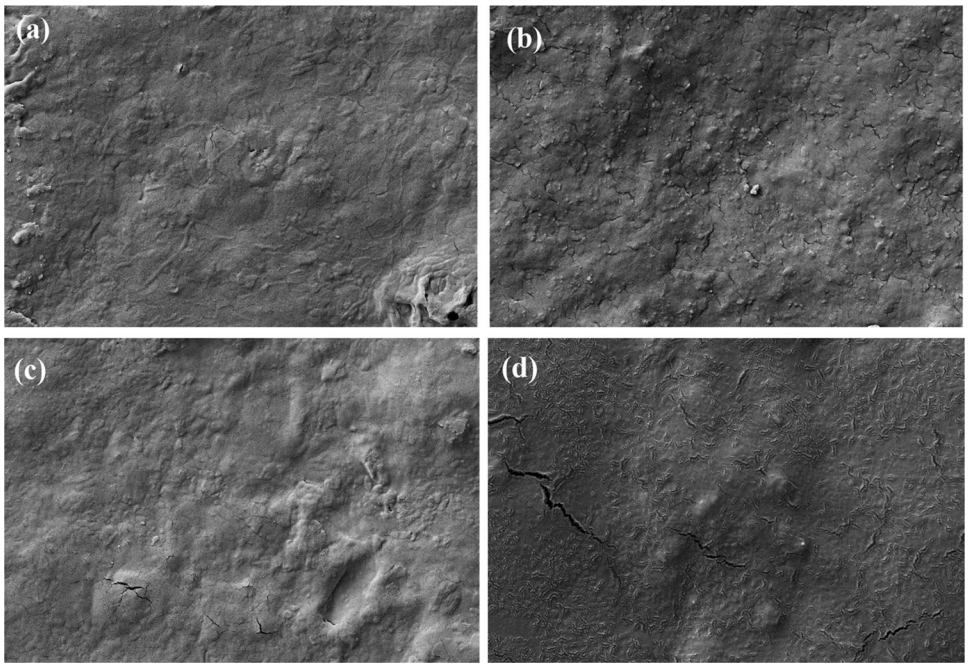

Fig. 11 The field emission scanning electron microscopy images (**a**) OPP, (**b**) OPP/Cr_2O_3, (**c**) OPP/AG, and (**d**) OPP/Cr_2O_3/AG

nanoparticles. Martins et al. [41] reported that films based on the carrageenan and lacuste gum had a uniform and dense surface and the addition of clay nanoparticles increased the roughness of the samples. Moreover, the addition of TiO_2 nanoparticles to films based on carrageenan gum, Xanthan Gum, and Gellan gum, caused the roughness of the sample [40].

FT-IR Test

FT-IR analysis is a useful and practical method to study and identify the intra-molecular interactions of the film samples. FT-IR spectra of the film samples are provided in Fig. 12. The peaks of the film are in the range of 600 cm^{-1} to 4000 cm^{-1}. The FT-IR spectra of the control films were almost similar to other film samples and there was no significant change in their functional groups. Meanwhile, there was no new peak in the film samples, indicating no change in the pectin-based film of the orange peel comprising gum arabic and nanoparticles. Overall, the position and severity of changed peaks are related to the interaction between nanoparticles and gum arabic with a polymer matrix. The peak index in 325 cm^{-1} reveals the tensile vibrations of O–H and CH_2–OH groups, which is related to the presence of starch, glycerol, and water compounds. Besides, the peak at 2923 cm^{-1} is related to the C–H alkankins and compounds in the polymer film matrix [42]. In this way, the absorbed bands of 2870–2960 cm^{-1} are attributed to the symmetric and asymmetric C=H groups [42, 43]. The peak in the range of 1605 cm^{-1} is related to the N–H Amide groups. Moreover, the absorption band in 1740 cm^{-1} represents the presence of tensile bonding C=O in the Amide groups [44]. The peaks at 1603–1605 cm^{-1} are due to carboxylic acid stretch bond. The absorption peak in the range of 1410 cm^{-1} is related to the vibrational group of O=H. Meanwhile, the absorption peak in the range of 1200 cm^{-1} to 1350 cm^{-1} represents the existence of the C–O tensile group in the Polysaccharide complex. The peak existing in the range of 1015 cm^{-1} to 1950 cm^{-1} denotes C=O tensile and vibrating groups. Moreover, the peaks observed in the range of 650 cm^{-1} to 950 cm^{-1} are related to the C=C and C–H bonding of the aromatic ring [45]. Overall, the addition of gum arabic and Cr_2O_3 NPs did not create a new peak in the FT-IR spectra.

X-Ray Diffraction Test (XRD)

The X-ray diffraction pattern is utilized to investigate the crystalline behavior of biodegradable films and their morphological properties [23]. The structure of compound films containing gum and nanoparticles was compared with the control sample (RNU 13) using the XRD test, which is shown in Fig. 13. The XRD spectrum of the film indicated that the films in 2θ of 12.3, 15.8, and 24.5 have sharp peaks, indicating the existence of crystalline structures in these films. Besides, those peaks with relatively broad heads in 2θ of 8 and 12, indicate the existence of an amorphous structure or irregularity in the film.

By adding gum arabic in sample 12, the peak of $2\theta = 12.3$ was removed while the peak height of $2\theta = 15.8$ was decreased. Meanwhile, the head of peak $2\theta = 8$ was also relatively wider. All these changes including reduced crystalline structure, the presence of crystals, and the

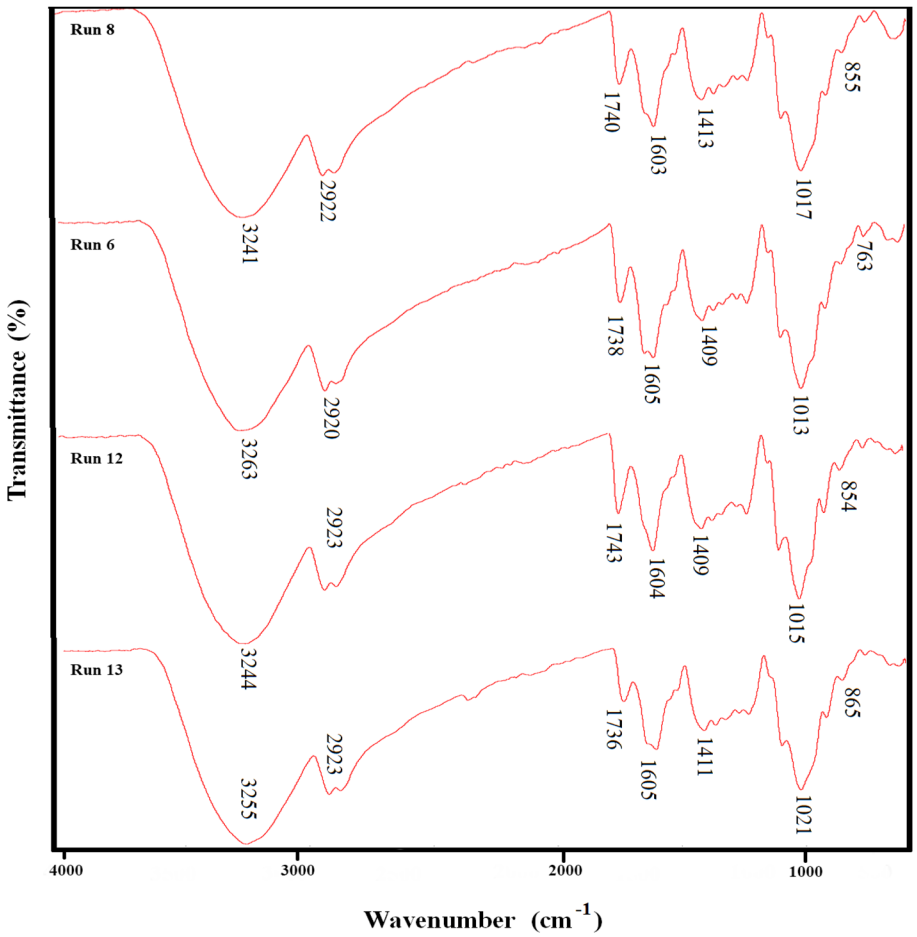

Fig. 12 The FT-IR spectroscopy (RUN 13) OPP, (RUN 6) OPP/Cr_2O_3, (RUN12) OPP/AG and (RUN 8) OPP/Cr_2O_3/AG

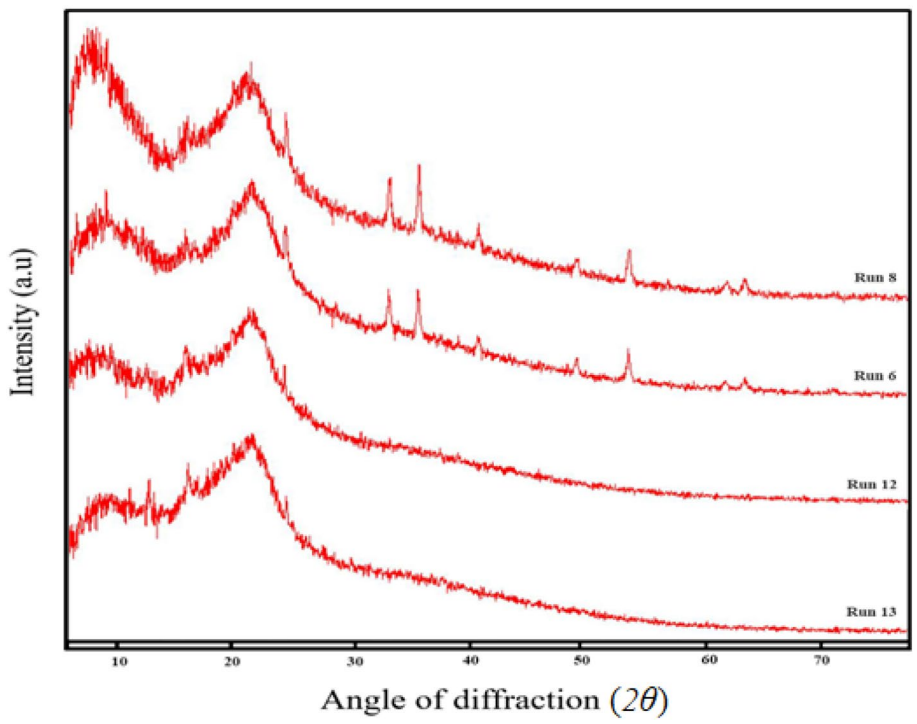

Fig. 13 The XRD curve (RUN 13) curve OPP, (Run 6) OPP/Cr_2O_3, (RUN12) OPP/AG, and (RUN 8) OPP/Cr_2O_3/AG

increased amorphous structure in the film structure are caused by gum arabic, as compared to the control sample. In the XRD spectrum of samples 6 with the highest percentage of nanoparticles and Arab gum, some new peaks in 2θ of 33.7, 36.2, 41.6, 50.3, 58.9, 63.5, and 65 are created. All these sharp peaks indicate crystallization and the formation of new crystals in sample 6, as compared to sample 13 as a result of the crystallization of nanoparticles added to the film structure.

In sample 8 with the highest percentage of gum and nanoparticles, in comparison with sample 13, a displacement was created in the peak from $2\theta = 8$ to $2\theta = 7$, such that the height of this peak was increased, indicating an increase in the crystallization degree of this sample, as compared to sample 13. In comparison with sample 6, a shift was created in sample 8 from $2\theta = 58.9$ to $2\theta = 54.8$, in which the height of the peak was increased. Furthermore, in 2θ of 33.7, 36.2, and 41.6, the height of the peaks was increased, while at $2\theta = 50.3$, the height of the peak was decreased. Overall, the crystallization degree of sample 8 was more than other tested samples, indicating that the addition of gum arabic and nanoparticles simultaneously caused new crystals, finally increasing the crystallization degree of the film.

Thermogravimetric Analysis (TGA)

TGA analysis is employed to investigate the thermal stability of the films. TGA and DTG thermal diagrams are provided in Fig. 14. In all film samples, the initial weight drop was observed at 70–120 °C because of the evaporation of moisture from the surface of the films [38]. The next weight drop was observed at around 150–250 °C because of the thermal decomposition of polymer and glycerol evaporation used as a plasticizer [46].

In this regard, similar results were proposed by Slavutsky et al. [47] for the film based on Montmorillonite nanoparticles and BREA gum. The maximum decomposition temperature specified from the temperature peak of the DTG curve is 213 °C for the control and film samples containing 5% gum arabic, whereas it is 225 °C for film samples containing 3% of the chromium oxidized nanoparticles, gum, and nanoparticles. As can be observed, by adding the nanoparticles, the maximum decomposition temperature increases, as compared to the film samples without the nanoparticles.

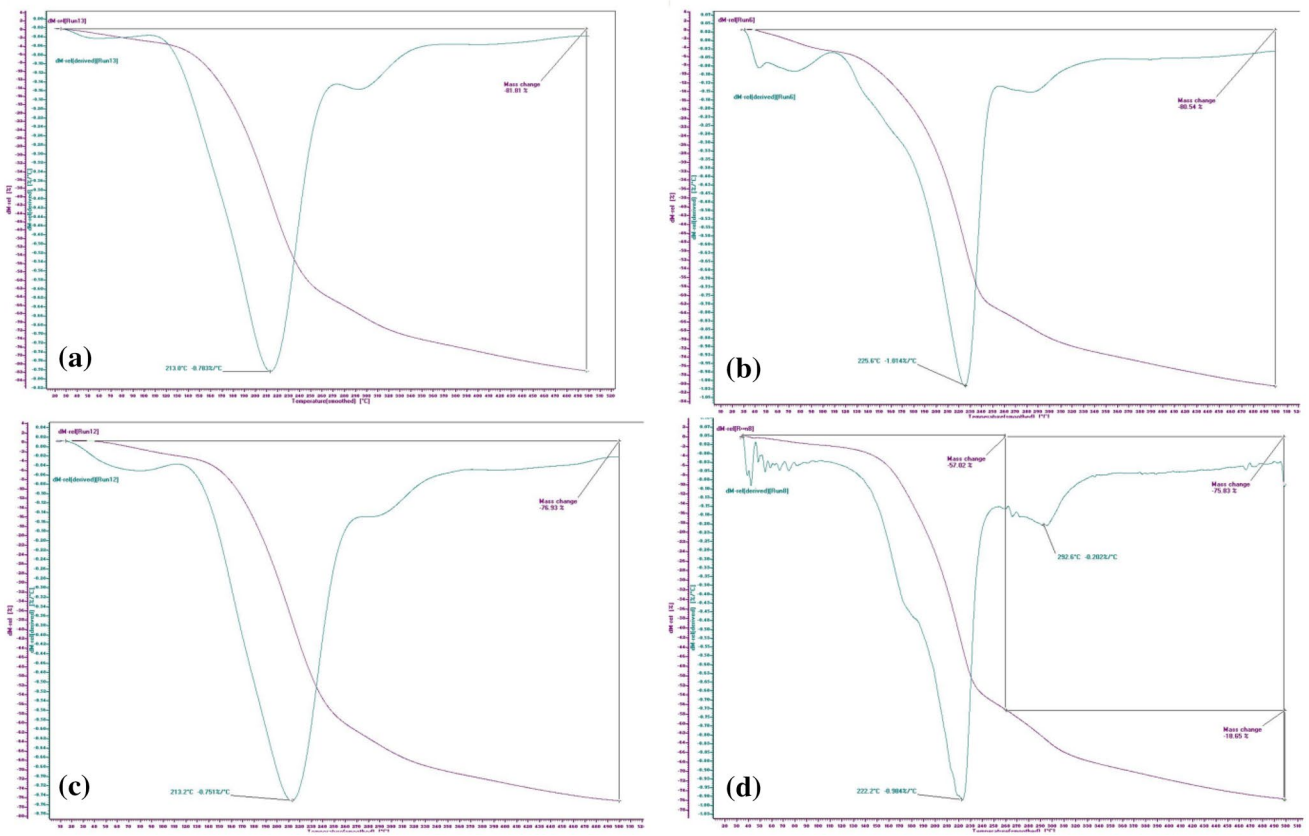

Fig. 14 The TGA curve of (**A**) OPP, (**B**) OPP/Cr_2O_3, (**C**) OPP/AG and (**D**) OPP/Cr_2O_3/AG

Furthermore, these results indicate that the thermal stability of orange peel film increases by adding the Cr_2O_3 NPs. Such behavior is likely due to the increased bending in the path of gas emissions as well as the restriction of oxygen and gases emission from the pyrolysis [47]. Oun and Rhim [39] proposed similar results reporting that the addition of zinc oxide nanoparticles to Carrageenans-based films increased the stability of films.

Investigating Antimicrobial Properties of Films

The disk diffusion method was employed to specify the antimicrobial properties of gum and Cr_2O_3 NPs. In this technique, a piece of antimicrobial film is placed in a solid culture medium containing the target microorganisms. After incubation at a specific temperature, the bright halo around the film represents the emission of the antimicrobial agent from the film and thus inhibition of the target microorganisms' growth. The disk diffusion method simulates packaging the food, indicating the performance of the film in contact with the contaminated surfaces as well as the immigration of the antimicrobial agent from the film to food [48].

The results of antimicrobial activity of gum and nanoparticles samples are illustrated in comparison with the control sample on the gram-positive bacteria of *S. aureus* and gram-negative bacteria of *E. coli* in Fig. 15. As can be observed, the control sample does not show the antimicrobial properties against both bacteria, and the halo is not observed around the film disk. Based on the obtained image, with the addition of gum and nanoparticles, the growth halo was observed around the films, indicating the release of antimicrobial agents. Nevertheless, as seen, the most halo was created in sample 8. However, there was no synergistic effect of gum and nanoparticles to destruct the tested microorganisms (Table 2).

Moreover, as seen, adding gum alone did not have a specific antimicrobial effect on the gram-negative bacteria of *E. coli*, which can be due to the presence of liposaccharide walls around the Peptidoglycan wall of gram-negative bacteria resulting in more bacterial resistance against the antibacterial agents [49]. The destruction of microorganisms due to the addition of nanoparticles can be associated with the leakage of intracellular materials by the holes generated on the cell wall. These holes are formed by oxidation of wall liposaccharides of cells owing to the nanoparticles-caused changes and differences.

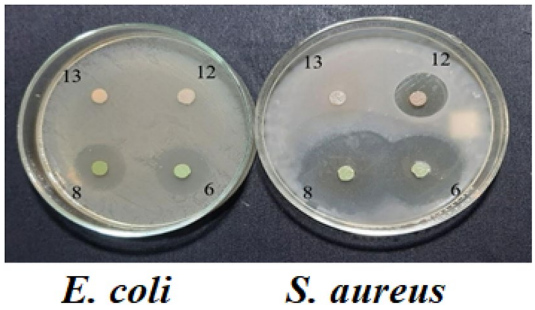

Fig. 15 The images of antimicrobial properties of films (RUN 13) OPP, (RUN 6) OPP/ Cr_2O_3, (RUN12) OPP/AG, and (RUN 8) OPP/ Cr_2O_3/AG

Table 2 The results of the microbial test of films based on orange peel and gum arabic

Sample	Diameter of non-growth area (mm)	
	S. aureus	*E. coli*
OPP	0.00 ± 0.00^{c}	0.00 ± 0.00^{b}
OPP/AG	19.59 ± 1.24^{b}	0.00 ± 0.00^{b}
OPP/Cr_2O_3	33.03 ± 1.34^{a}	20.42 ± 1.64^{a}
OPP/Cr_2O_3/AG	36.30 ± 2.30^{a}	18.99 ± 1.02^{a}

Different letters in each column indicate the significance at the level of $p < 0.05$

Conclusion

In this paper, OPP was utilized as an available, abundant, and cheap substance, compared to gum arabic to prepare the biodegradable films. Examining these films indicated that they had mechanical properties, inhibition, and good water solubility. The results revealed that the film solubility decreased by increasing the percentage of gum and Cr_2O_3 NPs. Furthermore, by adding gum arabic and nanoparticles, the tensile strength parameter had a significant increase, as compared to the control sample, which could be associated with the creation of appropriate interactions between film matrix and additive materials (such as gum arabic and Cr_2O_3 NPs). Besides, the creation of new hydrogen bonding increased the parameter. Moreover, the transparency of the films increased significantly by increasing the percentage of gum. The antimicrobial properties of the films increased significantly by increasing the nanoparticle percentage. Furthermore, the results of X-ray diffraction analysis confirmed a decreased crystalline structure and increased amorphous structure because of the addition of gum arabic.

Author Contribution SP and SG: Conceptualization, methodology. SG and SA: Data analysis, writing-original draft preparation. SG: investigation. PA: antimicrobial test. SP and SA: supervision. SA: software, validation. SG, SP and SA: writing-reviewing and editing.

References

1. Gholam-Zhiyan A, Amiri S, Rezazadeh-Bari M, Pirsa S (2021) Stability of *Bacillus coagulans* IBRC-M 10807 and *Lactobacillus plantarum* PTCC 1058 in milk proteins concentrate (MPC)-based edible film. J Packag Technol Res 5(1):11–22
2. Gennadios A (ed) (2002) Protein-based films and coatings. CRC Press, Boca Raton
3. Giménez B, Gómez-Estaca J, Alemán A, Gómez-Guillén MC, Montero MP (2009) Improvement of the antioxidant properties of squid skin gelatin films by the addition of hydrolysates from squid gelatin. Food Hydrocoll 23(5):1322–1327
4. Pirsa S, Aghbolagh Sharifi K (2020) A review of the applications of bioproteins in the preparation of biodegradable films and polymers. J Chem Lett 1(2):47–58
5. Amiri S, Rezazad Bari L, Malekzadeh S, Amiri S, Mostashari P, Ahmadi Gheshlagh P (2021) Effect of Aloe vera gel-based active coating incorporated with catechin nanoemulsion and calcium chloride on postharvest quality of fresh strawberry fruit. J Food Process Preserv. https://doi.org/10.1111/jfpp.15960
6. Amiri S, Saray FR, Rezazad-Bari L, Pirsa S (2021) Optimization of extraction and characterization of physicochemical, structural, thermal, and antioxidant properties of mucilage from Hollyhock's root: a functional heteropolysaccharide. J Food Measur Character 15(3):2889–2903
7. Verbeken D, Dierckx S, Dewettinck K (2003) Exudate gums: occurrence, production, and applications. Appl Microbiol Biotechnol 63(1):10–21
8. Sciarini LS, Maldonado F, Ribotta PD, Pérez GT, León AE (2009) Chemical composition and functional properties of *Gleditsia triacanthos* gum. Food Hydrocoll 23(2):306–313
9. Xu T, Gao C, Feng X, Huang M, Yang Y, Shen X, Tang X (2019) Cinnamon and clove essential oils to improve physical, thermal and antimicrobial properties of chitosan-gum arabic polyelectrolyte complexed films. Carbohyd Polym 217:116–125
10. Shanthilal J, Bhattacharya S (2017) Frying of rice flour dough strands containing gum Arabic: texture, sensory attributes and microstructure of products. J Food Sci Technol 54(5):1293–1303
11. Baron RD, Pérez LL, Salcedo JM, Córdoba LP, do Amaral Sobral PJ (2017) Production and characterization of films based on blends of chitosan from blue crab (*Callinectes sapidus*) waste and pectin from Orange (*Citrus sinensis* Osbeck) peel. Int J Biol Macromol 98:676–683
12. Taghavi Kevij H, Salami M, Mohammadian M, Khodadadi M, Emam-Djomeh Z (2021) Mechanical, physical, and bio-functional properties of biopolymer films based on gelatin as affected by enriching with orange peel powder. Polym Bull 78(8):4387–4402
13. Terzioğlu P, Güney F, Parın FN, Şen İ, Tuna S (2021) Biowaste orange peel incorporated chitosan/polyvinyl alcohol composite films for food packaging applications. Food Packag Shelf Life 30:100742
14. Rathinavel S, Saravanakumar SS (2020) Development and analysis of poly vinyl alcohol/orange peel powder biocomposite films. J Nat Fibers 18:2045–2054
15. Mascolo C, Marrone R, Palma A, Palma G (2013) Nutritional value of fish species. J Nutr Ecol Food Res 1(3):219–225
16. Asdagh A, Pirsa S (2020) Bacterial and oxidative control of local butter with smart/active film based on pectin/nanoclay/*Carum copticum* essential oils/β-carotene. Int J Biol Macromol 165:156–168
17. Pirsa S, Farshchi E, Roufegarinejad L (2020) Antioxidant/antimicrobial film based on carboxymethyl cellulose/gelatin/TiO_2–Ag nano-composite. J Polym Environ 28(12):3154–3163
18. Hassannia-Kolaee M, Khodaiyan F, Pourahmad R, Shahabi-Ghahfarrokhi I (2016) Development of ecofriendly bionanocomposite: whey protein isolate/pullulan films with nano-SiO_2. Int J Biol Macromol 86:139–144
19. Ghamari MA, Amiri S, Rezazadeh-Bari M, Rezazad-Bari L (2021) Physical, mechanical, and antimicrobial properties of active edible film based on milk proteins incorporated with *Nigella sativa* essential oil. Polym Bull. https://doi.org/10.1007/s00289-021-03550-y
20. Zhu JY, Tang CH, Yin SW, Yang XQ (2018) Development and characterization of novel antimicrobial bilayer films based on Polylactic acid (PLA)/Pickering emulsions. Carbohyd Polym 181:727–735
21. Jouki M, Khazaei N, Ghasemlou M, HadiNezhad M (2013) Effect of glycerol concentration on edible film production from cress seed carbohydrate gum. Carbohyd Polym 96(1):39–46
22. Wong SM, Zulkifli MZA, Nordin D, Teow YH (2021) Synthesis of cellulose/nano-hydroxyapatite composite hydrogel absorbent for removal of heavy metal ions from palm oil mill effluents. J Polym Environ 29:1–14
23. Salas-Valero LM, Tapia-Blácido DR, Menegalli FC (2015) Biofilms based on canihua flour (Chenopodium Pallidicaule): design and characterization. Quim Nova 38(1):14–21
24. Bazargani-Gilani B, Aliakbarlu J, Tajik H (2015) Effect of pomegranate juice dipping and chitosan coating enriched with *Zataria multiflora Boiss* essential oil on the shelf-life of chicken meat during refrigerated storage. Innov Food Sci Emerg Technol 29:280–287
25. Bahrami A, Mokarram RR, Khiabani MS, Ghanbarzadeh B, Salehi R (2019) Physico-mechanical and antimicrobial properties of tragacanth/hydroxypropyl methylcellulose/beeswax edible films reinforced with silver nanoparticles. Int J Biol Macromol 129:1103–1112
26. Oleyaei SA, Zahedi Y, Ghanbarzadeh B, Moayedi AA (2016) Modification of physicochemical and thermal properties of starch films by incorporation of TiO_2 nanoparticles. Int J Biol Macromol 89:256–264
27. Li LH, Deng JC, Deng HR, Liu ZL, Li XL (2010) Preparation, characterization and antimicrobial activities of chitosan/Ag/ZnO blend films. Chem Eng J 160(1):378–382
28. Pirsa S (2020) Biodegradable film based on pectin/Nano-clay/methylene blue: structural and physical properties and sensing ability for measurement of vitamin C. Int J Biol Macromol 163:666–675
29. Rezaei M, Pirsa S, Chavoshizadeh S (2019) Photocatalytic/antimicrobial active film based on wheat gluten/ZnO nanoparticles. J Inorg Organomet Polym Mater 30:2654
30. Sui C, Zhang W, Ye F, Liu X, Yu G (2016) Preparation, physical, and mechanical properties of soy protein isolate/guar gum composite films prepared by solution casting. J Appl Polym Sci. https://doi.org/10.1002/app.43382
31. Khoirunnisa AR, Joni IM, Panatarani C, Rochima E, Praseptiangga D (2018) UV-screening, transparency and water barrier properties of semi refined iota carrageenan packaging film incorporated with ZnO nanoparticles. In AIP conference proceedings, vol 1927, no. 1. AIP Publishing LLC, p 030041
32. Tunç S, Duman O (2010) Preparation and characterization of biodegradable methyl cellulose/montmorillonite nanocomposite films. Appl Clay Sci 48(3):414–424
33. Baek SK, Song KB (2018) Development of Gracilaria vermiculophylla extract films containing zinc oxide nanoparticles and their application in smoked salmon packaging. LWT 89:269–275
34. Anaya-Esparza LM, Ruvalcaba-Gómez JM, Maytorena-Verdugo CI, González-Silva N, Romero-Toledo R, Aguilera-Aguirre S, Pérez-Larios A (2020) Chitosan-TiO_2: a versatile hybrid composite. Materials 13(4):811
35. Jabraili A, Pirsa S, Pirouzifard MK, Amiri S (2021) Biodegradable nanocomposite film based on gluten/silica/calcium chloride:

physicochemical properties and bioactive compounds extraction capacity. J Polym Environ 29:2557–2571
36. He Q, Zhang Y, Cai X, Wang S (2016) Fabrication of gelatin–TiO_2 nanocomposite film and its structural, antibacterial and physical properties. Int J Biol Macromol 84:153–160
37. Farshchi E, Pirsa S, Roufegarinejad L, Alizadeh M, Rezazad M (2019) Photocatalytic/biodegradable film based on carboxymethyl cellulose, modified by gelatin and TiO_2-Ag nanoparticles. Carbohyd Polym 216:189–196
38. Kanmani P, Rhim JW (2014) Physicochemical properties of gelatin/silver nanoparticle antimicrobial composite films. Food Chem 148:162–169
39. Oun AA, Rhim JW (2017) Carrageenan-based hydrogels and films: effect of ZnO and CuO nanoparticles on the physical, mechanical, and antimicrobial properties. Food Hydrocoll 67:45–53
40. Balasubramanian R, Kim SS, Lee J, Lee J (2019) Effect of TiO2 on highly elastic, stretchable UV protective nanocomposite films formed by using a combination of k-Carrageenan, xanthan gum and gellan gum. Int J Biol Macromol 123:1020–1027
41. Martins JT, Bourbon AI, Pinheiro AC, Souza BW, Cerqueira MA, Vicente AA (2013) Biocomposite films based on κ-carrageenan/locust bean gum blends and clays: physical and antimicrobial properties. Food Bioprocess Technol 6(8):2081–2092
42. Piñeros-Hernandez D, Medina-Jaramillo C, López-Córdoba A, Goyanes S (2017) Edible cassava starch films carrying rosemary antioxidant extracts for potential use as active food packaging. Food Hydrocoll 63:488–495
43. Choo K, Ching YC, Chuah CH, Julai S, Liou NS (2016) Preparation and characterization of polyvinyl alcohol-chitosan composite films reinforced with cellulose nanofiber. Materials 9(8):644
44. Li H, Pu Y, Kumar R, Ragauskas AJ, Wyman CE (2014) Investigation of lignin deposition on cellulose during hydrothermal pretreatment, its effect on cellulose hydrolysis, and underlying mechanisms. Biotechnol Bioeng 111(3):485–492
45. Lozano-Navarro JI, Díaz-Zavala NP, Velasco-Santos C, Melo-Banda JA, Páramo-García U, Paraguay-Delgado F et al (2018) Chitosan-starch films with natural extracts: physical, chemical, morphological and thermal properties. Materials 11(1):120
46. Shankar S, Teng X, Rhim JW (2014) Properties and characterization of agar/CuNP bionanocomposite films prepared with different copper salts and reducing agents. Carbohyd Polym 114:484–492
47. Slavutsky AM, Bertuzzi MA, Armada M, García MG, Ochoa NA (2014) Preparation and characterization of montmorillonite/brea gum nanocomposites films. Food Hydrocoll 35:270–278
48. Genskowsky E, Puente LA, Pérez-Álvarez JA, Fernandez-Lopez J, Muñoz LA, Viuda-Martos M (2015) Assessment of antibacterial and antioxidant properties of chitosan edible films incorporated with maqui berry (Aristotelia chilensis). LWT-Food Sci Technol 64(2):1057–1062
49. Burt S (2004) Essential oils: their antibacterial properties and potential applications in foods—a review. Int J Food Microbiol 94(3):223–253